# Improvement of blood vessel visualization in laser speckle contrast imaging using adaptive processing methods

E. Morales-Vargas, H. Peregrina-Barreto & J.C. Ramirez-San-Juan
Instituto Nacional de Astrofísica, Óptica y Electrónica (Puebla, México)

## 1.- Introduction

Microvasculature visualization (MV) aims to locate and visualize superficial and deep blood vessels in biomedical images. Widely used in neuroscience, dermatology, or ophthalmology to diagnose, treat, and track some diseases, such as the port-wine stain birthmarks, retinopathy, among others [1].

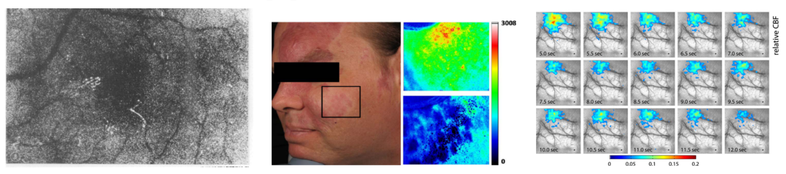


(a) (b) (c)

**Figure 1:** Applications of MV for (a) retinal blood flow, (b) port-wine treatment and (c) cerebral activation.

Laser Speckle Contrast Imaging (LSCI) allows the visualization of microvasculature by analyzing particle movement in a Raw Speckle Image (RSI) through a Contrast Image (CI) [2].

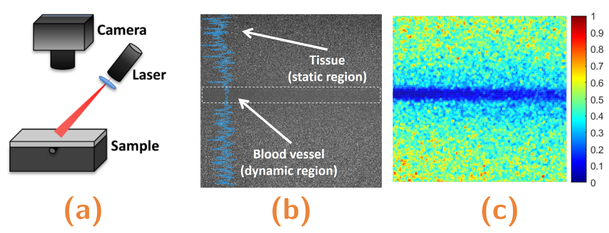


(a) (b) (c)

**Figure 2:** (a) Laser speckle imaging setupRegan2014, (b) raw speckle image and (c) contrast image of (b).

Traditional methods use analysis windows of fixed size to attenuate noise in a CI [3, 4, 5].

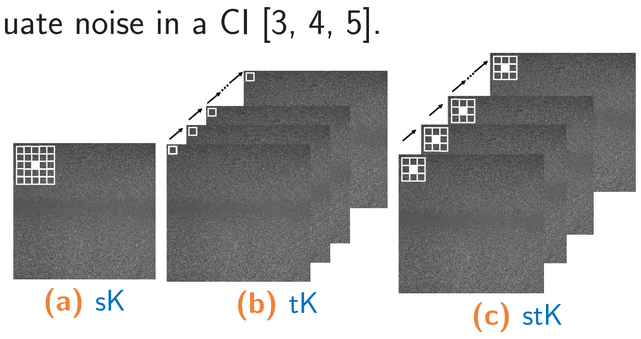

(a) sK (b) tK (c) stK

**Figure 3:** Traditional methods of LSCI: (a) sK, (b) tK, and (c) stK.

Recent research has demonstrated that anisotropic approaches reach significant improvement in noise attenuation [6].

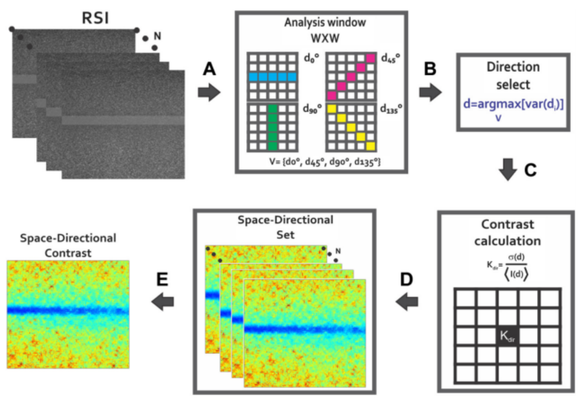


**Figure 4:** Space-directional contrast representation (sdK).

But high depth is still an issue to address.

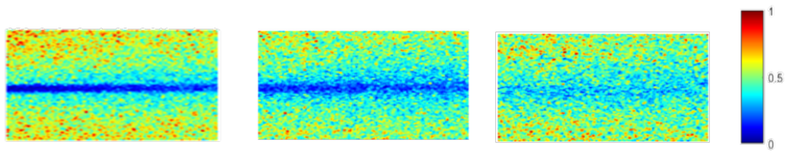


**Figure 5:** Averaged spatial contrast (asK) varying the deep of the blood vessel from 0, 400, and 900 $\mu m$ from left to right.

This work aims to reduce the noise in CIs by computing them through adaptive analysis windows that change their size and shape according to the local characteristics of the analyzed region. The adaptive property allows selecting the pixels involved in the contrast calculation, including more pixels from the region of interest (blood vessel) and avoiding noisy pixels.

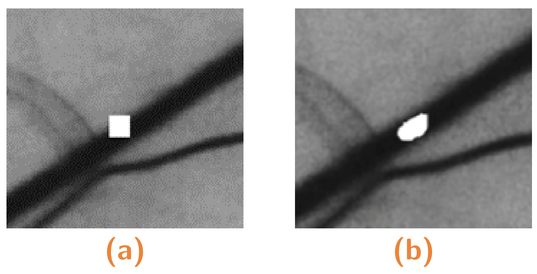

(a) (b)

**Figure 6:** Example of an analysis window (white region) processing the contrast value over a blood vessel (black) in a patch of a LSCI image in the torso of a rat: (a) traditional approach (fixed shape and size) and (b) an adaptive approach.

## 2.- Proposed approach

The proposed approach selects the pixels involved in the contrast calculation for each pixel in the RSI using a region growing process.

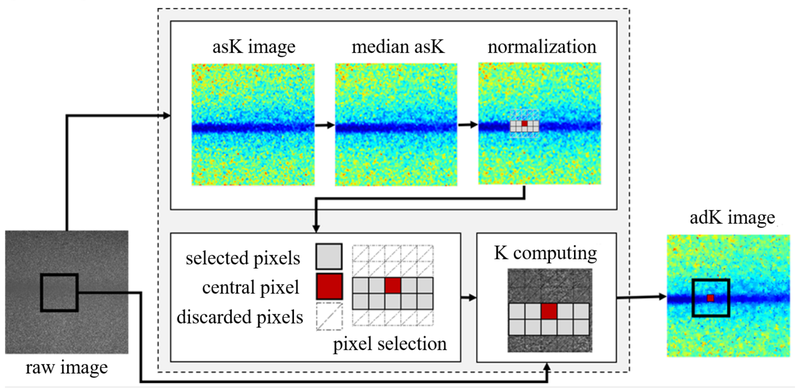


**Figure 7:** Flowchart of the proposed approach.

The pixel selection process was improved using a selection before the analyzed pixel, as shown in the algorithm from lines 6 to 10.

1: **procedure** ADAPTIVE CONTRAST($I$,$r$,$tr$,$wf$)
2: $R \leftarrow saKofI$
3: $R \leftarrow$ median filter of $R$ with size $wf$
4: $R \leftarrow$ 95% percentile normalization
5: **for each** pixel $x \in$ R **do**
6: **if** $x \in S^r_{x-1}$ **then**
7: Update $S^r_x$ using $S^r_{x-1}$
8: **else**
9: Compute $S^r_x$ using $tr$
10: **end if**
11: $P \leftarrow \{pp \in I : S^d_p(pp) = 1\}$
12: $K(p) \leftarrow \frac{\sqrt{\sigma^P}}{\mu^P}$
13: **end for**
14: **end procedure**

**Figure 8:** Algorithm for adaptive processing of CI.

## 2.- Experiments and quantitative results

The RSI images used for testing have dimensions of $344 \times 329$ and $280 \times 288$ for straight and bifurcated in-vitro blood vessels; the in-vivo images have dimensions of $1040 \times 1392$ [7].

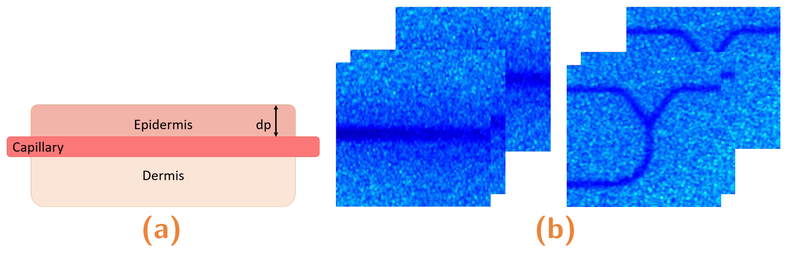


(a) (b)

**Figure 9:** a) used phantom to simulate depths in the *in-vitro* RSIs. b) simulated images with depths of 0, 200, 400, 500, 700, 900 $\mu m$.

The parameters used by the algorithm were $w = 13$, filter size $= 11$ and $tr = 0.15$.

**Table 1:** CNR per approach.

| depth ($\mu m$) | CNR per contrast approach aK | sK | saK | sdK | stK | **adK** |
|---|---|---|---|---|---|---|
| 0 | 1.24 | 2.48 | 2.50 | 1.76 | 2.50 | **3.5** |
| 200 | 1.08 | 2.20 | 2.29 | 1.55 | 2.29 | **3.29** |
| 300 | 0.84 | 1.89 | 1.97 | 1.27 | 1.95 | **2.17** |
| 400 | 0.93 | 1.90 | 1.92 | 1.35 | 1.92 | **2.81** |
| 500 | 0.61 | 1.34 | 1.60 | 0.91 | 1.60 | **2.49** |
| 600 | 0.63 | 1.29 | 1.33 | 0.89 | 1.33 | **1.04** |
| 700 | 0.49 | 1.09 | 1.21 | 0.73 | 1.21 | **2.00** |
| 900 | 0.47 | 1.04 | 1.04 | 0.69 | 1.04 | **1.73** |
| *in-vivo* | 1.67 | 1.96 | 2.90 | 1.43 | 2.84 | **2.94** |
| total | 0.89 | 1.69 | 1.86 | 1.18 | 1.85 | **2.66** |
| std | 0.37 | 0.48 | 0.58 | 0.36 | 0.57 | **0.59** |

**Table 2:** JI per approach.

| depth ($\mu m$) | JI per contrast approach aK | sK | saK | sdK | stK | **adK** |
|---|---|---|---|---|---|---|
| 0 | 0.63 | 0.75 | 0.76 | 0.73 | 0.76 | **0.75** |
| 200 | 0.54 | 0.72 | 0.75 | 0.71 | 0.75 | **0.81** |
| 300 | 0.36 | 0.62 | 0.62 | 0.52 | 0.62 | **0.70** |
| 400 | 0.31 | 0.70 | 0.68 | 0.64 | 0.68 | **0.67** |
| 500 | 0.00 | 0.60 | 0.65 | 0.39 | 0.64 | **0.73** |
| 600 | 0.00 | 0.56 | 0.56 | 0.23 | 0.56 | **0.48** |
| 700 | 0.00 | 0.49 | 0.53 | 0.05 | 0.53 | **0.65** |
| 900 | 0.00 | 0.42 | 0.42 | 0.03 | 0.42 | **0.47** |
| *in-vivo* | 0.54 | 0.58 | 0.62 | 0.55 | 0.61 | **0.62** |
| total | 0.26 | 0.58 | 0.61 | 0.40 | 0.61 | **0.63** |
| std | 0.24 | 0.11 | 0.10 | 0.26 | 0.10 | **0.11** |

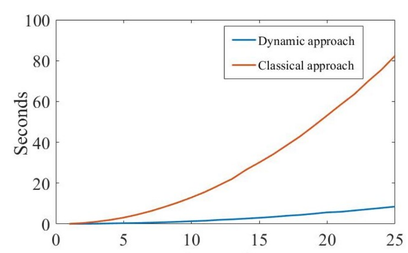


**Figure 10:** Processing time of the proposed algorithm with a max analysis window of 15.

## 3.- Qualitative results

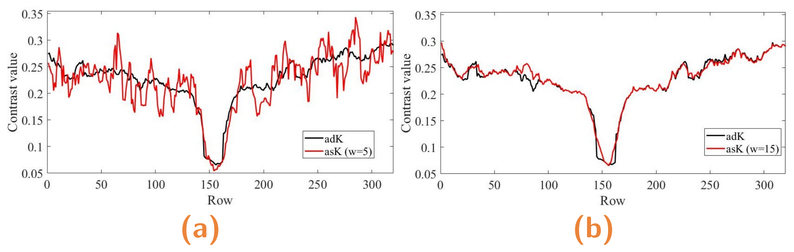


(a) (b)

**Figure 11:** Profile of an CI processed with the adaptive method (proposed), and an averaged spatial contrast with a) $w = 5$ and b) $w = 15$.

## 3.- Qualitative results (cont)

Column 600 was taken to perform a subjective noise analysis of an *in-vivo* CI.

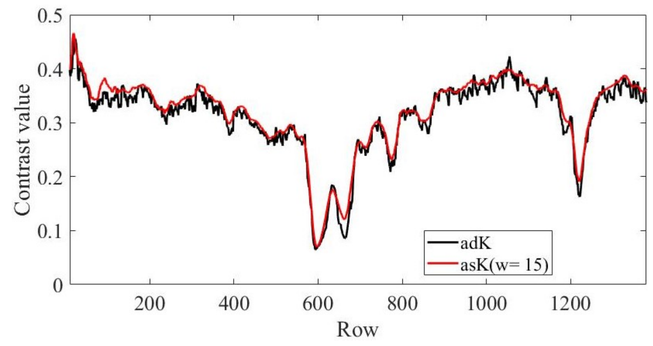


**Figure 12:** Slice of a CI, the noise is reduced in the adK approach.

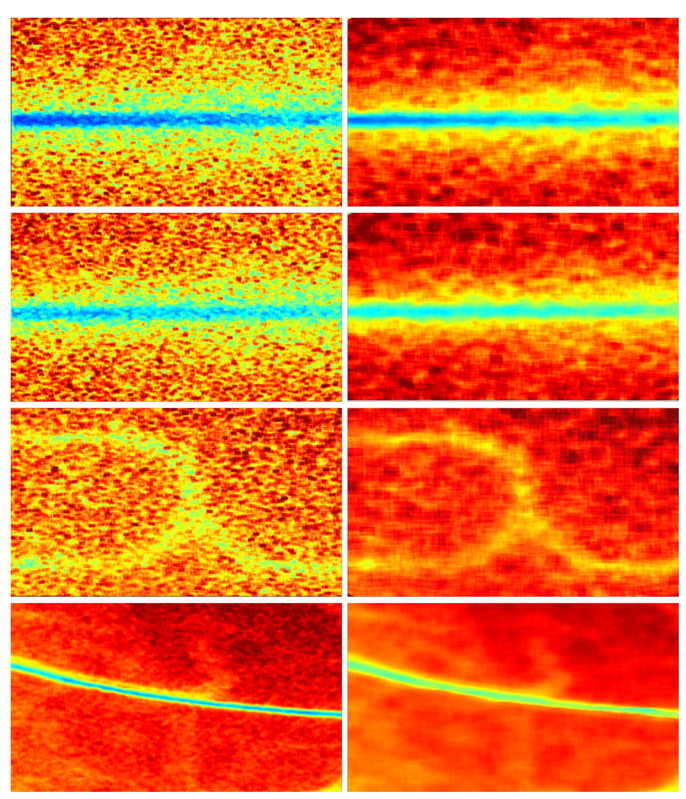

**Figure 13:** Images of CI processed with the spatial averaged approach using a standard window $w = 5$ (left) and the adK approach (right). As can be seen, with the proposed approach (adK) the contrast between regions was enhanced, and the noise level was reduced.

Segmentation results show that the adK method is more suitable for noise attenuation, which translates into less false-positive rates.

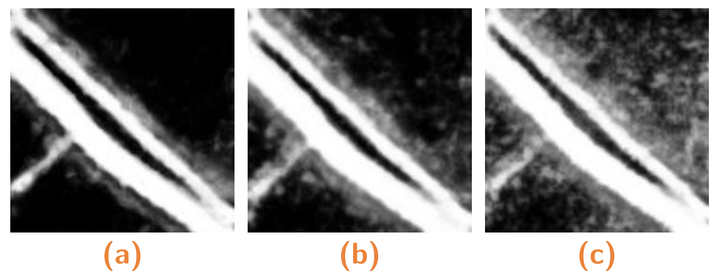

(a) (b) (c)

**Figure 14:** *In-vivo* Laser speckle probability maps. The brighter the region, the more likely the pixel to be a blood vessel: (a) adK, (b) asK with $w = 5$, and (c) tK

## 4.- Conclusions

- Obtained results suggest that the selection of pixels involved in the contrast calculation can improve the contrast between regions in LSCI.
- The proposed method can improve the segmentation of blood vessels in LSCI, increasing the JI by reducing the noise, which translates into a false positive rate reduction.
- With an updating of the pixel selection using the previously selected pixels, the time of adaptive processing can be reduced compared to the traditional method without the improvement.

## References

"Histograms of oriented gradients for human detection," vol. 1, pp. 886–893, 6 2005.

C. Regan, J. C. Ramirez-San-Juan, and B. Choi, "Photothermal laser speckle imaging.," *Optics letters*, vol. 39, pp. 5006–9, 9 2014.

C. Bernard, T. Wenbin, and J. Wangcun, "The Role of Laser Speckle Imaging in Port-Wine Stain Research: Recent Advances and Opportunities," vol. 4, no. 11, pp. 1–32, 2017.

M. S. D. Smith, E. F. Packulak, and M. G. Sowa, "Development of a laser speckle imaging system for measuring relative blood flow velocity," *Proceedings of SPIE - The International Society for Optical Engineering*, vol. 6343 I, no. September 2006, pp. TeraXion, Canada; Developpement economique Canada,, 2006.

J. D. Briers and A. F. Fercher, "Retinal blood-flow visualization by means of laser speckle photography.," *Investigative ophthalmology & visual science*, vol. 22, pp. 255–9, 2 1982.

C. Perez-Corona, "Space-directional Laser Speckle Contrast Imaging to Improve Blood Vessels Visualization," 2018.

B. Choi, N. M. Kang, and J. S. Nelson, "Laser speckle imaging for monitoring blood